Cell, Vol. 111, 791–802, December 13, 2002, Copyright ©2002 by Cell Press

Physical and Functional Interactions among Basic Chromosome Organizational Features Govern Early Steps of Meiotic Chiasma Formation

Yuval Blat,[2,4] Reine U. Protacio,[2,4] Neil Hunter,[3] and Nancy Kleckner[1]
Department of Molecular and Cellular Biology
Harvard University
Cambridge, MA 02138

Summary

Analysis of meiotic recombination by functional genomic approaches reveals prominent spatial and functional interactions among diverse organizational determinants. Recombination occurs between chromatin loop sequences; however, these sequences are spatially tethered to underlying chromosome axes via their recombinosomes. Meiotic chromosomal protein, Red1, localizes to chromosome axes; however, Red1 loading is modulated by R/G-bands isochores and thus by bulk chromatin state. Recombination is also modulated by isochore determinants: R-bands differentially favor double-strand break (DSB) formation but disfavor subsequent loading of meiotic RecA homolog, Dmc1. Red1 promotes DSB formation in both R- and G-bands and then promotes Dmc1 loading, specifically counteracting disfavoring R-band effects. These complexities are discussed in the context of chiasma formation as a series of coordinated local changes at the DNA and chromosome-axis levels.

Introduction

During meiotic prophase, replicated homologs identify one another and become progressively more intimately juxtaposed until they are connected along their entire lengths; they then separate, revealing a few remaining connections known as "chiasmata" (Figure 1A). Chiasmata are mechanically important to ensure bipolar alignment and regular segregation of homologs during the first (reductional) meiotic division.

Each chiasma corresponds to the site of a reciprocal exchange, or "crossover", at the DNA level, as shown cytologically by differential staining of sister chromatid chromatin (Figure 1B). Differential staining of the structural axes along which chromatin is organized reveals two further aspects of chiasmata: (1) reciprocal exchange also occurs between chromatid axes, which are morphologically continuous across chiasma sites; and (2) in accord with the fact that only one chromatid of each homolog participates in exchange, sister chromatid axes are locally separated at each chiasma (Figure 1C).

DNA recombination occupies most of prophase (Figure 1A). The process initiates via programmed double-strand breaks (DSBs) and, following a series of additional transitions, crossovers finally appear at about the onset of general homolog separation (Hunter and Kleckner, 2001; Allers and Lichten, 2001). Neither exchange at the structural level nor coordination of events at DNA and structural levels is understood. However, meiotic recombination complexes are spatially associated with their chromosome axes. This is clear at early/intermediate stages for RecA homolog-containing complexes that assemble on DSBs (Anderson et al., 1997; Franklin et al., 1999; Tarsounas et al., 1999) and related early recombination nodules (Figure 1D). Thereafter, recombinosomes are associated with the synaptonemal complex (SC), the structure that mediates the connection of homologs along their lengths at mid-prophase. Perhaps spatial association of recombinosomes with underlying chromosome axes mediates coordination between events at the DNA and axis levels (Discussion).

The basic structure of meiotic prophase chromosomes is defined from studies of pachytene SCs. Each chromatid is organized into a linear array of chromatin loops, the bases of which define a geometric axis that is elaborated by various proteins (Figure 1E, top); sister chromatids are closely conjoined as parallel cooriented linear loop-arrays, whose axes comprise a single morphological unit (Figure 1E, bottom; Zickler and Kleckner, 1999). The density of chromatin loops along chromosomes is evolutionarily conserved, with the bases of sister loops conjoined in dual loop modules (Zickler and Kleckner, 1999). Since basic prophase chromosome organization is probably established during S-phase, meiotic recombination may initiate and proceed entirely in the context of such cooriented linear loop arrays. It is not known exactly when recombinosome/axis association is first established or what its underlying organizational basis might be (von Wettstein, 1971; Zickler and Kleckner, 1999; van Heemst and Heyting, 2000).

Chiasma formation also varies domainally along chromosomes. For example, mammalian chromosome arms are composed of GC-rich "R-bands" and AT-rich "G-bands", which differ in their functional properties, e.g., higher and lower levels of gene expression, earlier and later DNA replication, and higher and lower levels meiotic crossovers (Holmquist, 1992; Saitoh and Laemmli, 1994; Zickler and Kleckner, 1999).

Here, we further investigate relationships between several aspects of chromosome organization and recombination (and thus, chiasma formation) using yeast as a model system. Yeast meiotic chromosomes share the universal cooriented sister linear loop structure (Dresser and Giroux, 1988; Zickler and Kleckner, 1999). In mitotic cells, cohesins bind to a series of locally AT-rich regions that correspond to the AT queue of the mammalian mitotic chromosome axis (Blat and Kleckner, 1999; Results). These and other observations (Peltari et al., 2001; Guacci et al., 1997) suggest that, during meiosis, cohesins define the basic cooriented linear loop array structure and its individual dual loop modules. Yeast chromosomes also have R-/G-band base composition isochores, analogous to those of mammalian

[1] Correspondence: kleckner@fas.harvard.edu
[2] Present address: Bristol-Myers Squibb, Wilmington, Delaware 19880.
[3] Present address: Center for Genetics and Development, Departments of Microbiology and Molecular and Cellular Biology, University of California, Davis, Davis, California 95616.
[4] These authors contributed equally to this work.

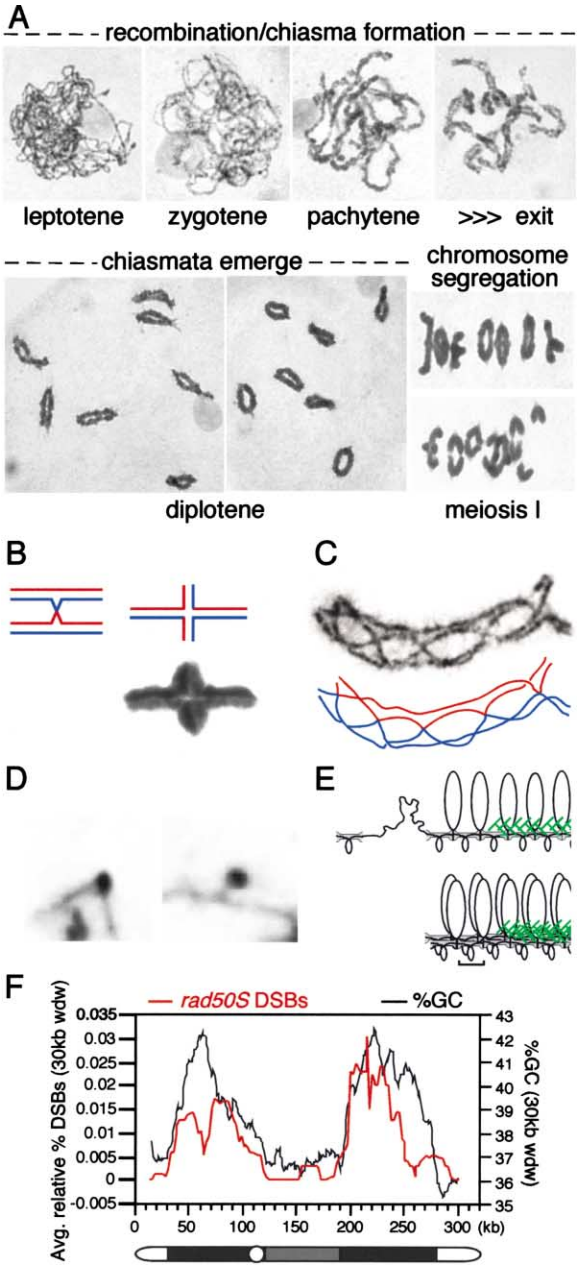

Figure 1. Meiotic Chromosome Axis and Chromosome III Features

(A) Meiotic stages from early prophase through the first (reductional) division as illustrated by images of fixed, stained rye chromosomes (photographs by D. Zickler, used with permission).

(B) Chiasmata represent sites of reciprocal exchange between non-sister chromatids of homologous chromosomes at the DNA/chromatin level. Two topological forms of a mono-chiasmate bivalent are St. Andrew's cross (left) and open Greek cross (top right). Exchange is revealed by differential staining of sister chromatid chromatin (bottom right, in *Locusta migratoria;* Tease, 1978; reprinted by permission from Nature *272*, 823–824; copyright 1978 Macmillan Publishers Ltd.).

(C) Local structural changes at chiasma sites. Diplotene bivalent of *Chorthippus parallelus* stained to reveal chromatid axes, which are exchanged and continuous across the exchange point with accompanying local separation of sister axes (Figure 2.3a of John, 1990; reprinted with the permission of Cambridge University Press).

(D) Leptotene chromosome conformations observed in plants. Round nodule associated with sharp bend in axis (left) leads to stick-and-ball configuration (center; from *Lycopersicon esculentum*; Stack and Anderson, 1986; reprinted by permission from Am. J. Bot. *73*, 264–281; copyright 1986 Botanical Society of America). Partner axis is then brought into close juxtaposition leading to inter-axis bridges (not shown). All configurations are thought to represent RecA homolog-containing recombinosomes that arise immediately following DSB formation (G.H. Jones, cited in Zickler and Heckner, 1999).

(E) Throughout meiotic prophase, each chromatid is organized into a linear array of loops (top). The bases of these loops define a geometric axis, which, as elaborated by proteins, comprises a structural axis. Sister chromatid linear loop arrays are cooriented and closely conjoined along their axes, which form a single morphological unit (bottom). Along the axis, gray units represent basic loop modules (e.g., cohesins); green represents other axis-associated proteins (e.g., Red1). The homolog axis comprises a linear array of "dual loop modules" (indicated by bracket).

(F) Meiotic DSB hotspots and base-composition isochores along chromosome III.

Meiotic DSBs at hot spots in a *rad50S* mutant strain (%DNA; red line; Baudat and Nicolas, 1997) and %GC sequence composition (black line), both averaged over an ~30 kb sliding window ("wdw"), as a function of chromosomal position (Experimental Procedures). Cartoon identifies the centromere (white circle), the two GC-rich isochores (R-bands-dark gray rectangles at 30–120 kb and 190–280 kb), the single AT-rich isochore (G-band-light gray rectangle at 120–190 kb) and the telomeres (white regions).

chromosomes, which emerge when average base composition is defined by a 30–50 kb sliding window (Sharp and Lloyd, 1993; Dujon, 1996). Chromosome III comprises two GC-rich isochores (R-bands) flanking a central AT-rich isochore (G-band; Figure 1F). Yeast R-bands also exhibit higher levels of both transcription (Petes, 2001) and meiotic DSBs (Baudat and Nicolas, 1997; Figure 1F; Results).

The current study utilizes chromatin immunoprecipitation (ChIP) plus a chromosome III microarray to define the localization of two key meiotic proteins, Red1 and Dmc1. Red1 is an abundant chromosomal protein, seen cytologically to occur in prominent patches along prophase chromosome axes (Smith and Roeder, 1997). Red1 is implicated in several aspects of recombination (Mao-Draayer et al. 1996; Rockmill and Roeder, 1988, 1990; Schwacha and Kleckner, 1997) and in structural aspects of prophase chromosomes, i.e., formation of silver-staining axial elements (AEs) and SC, and maintenance of intersister connections (Rockmill and Roeder, 1988, 1990; Smith and Roeder, 1997; Bailis and Roeder, 1998). Dmc1 is a meiosis-specific RecA homolog that loads onto the ends of newly formed DSBs (e.g., Shinohara et al., 2000). Positions of Dmc1 binding should mark DSB sites. The pattern of Dmc1 binding will also be sensitive to factors that influence its loading onto those DSBs. We have also reanalyzed the distribution of chromosome III DSBs that occur specifically at recombination hot spots (Baudat and Nicolas, 1997). Finally, we have examined the effects of eliminating Red1 for both DSB distribution and Dmc1 localization.

These studies reveal complex organizational and functional interplay among basic chromosomal determinants during meiotic prophase. Implications of these findings for chiasma formation and the relationship of chiasma formation to basic mitotic chromosome function are discussed.

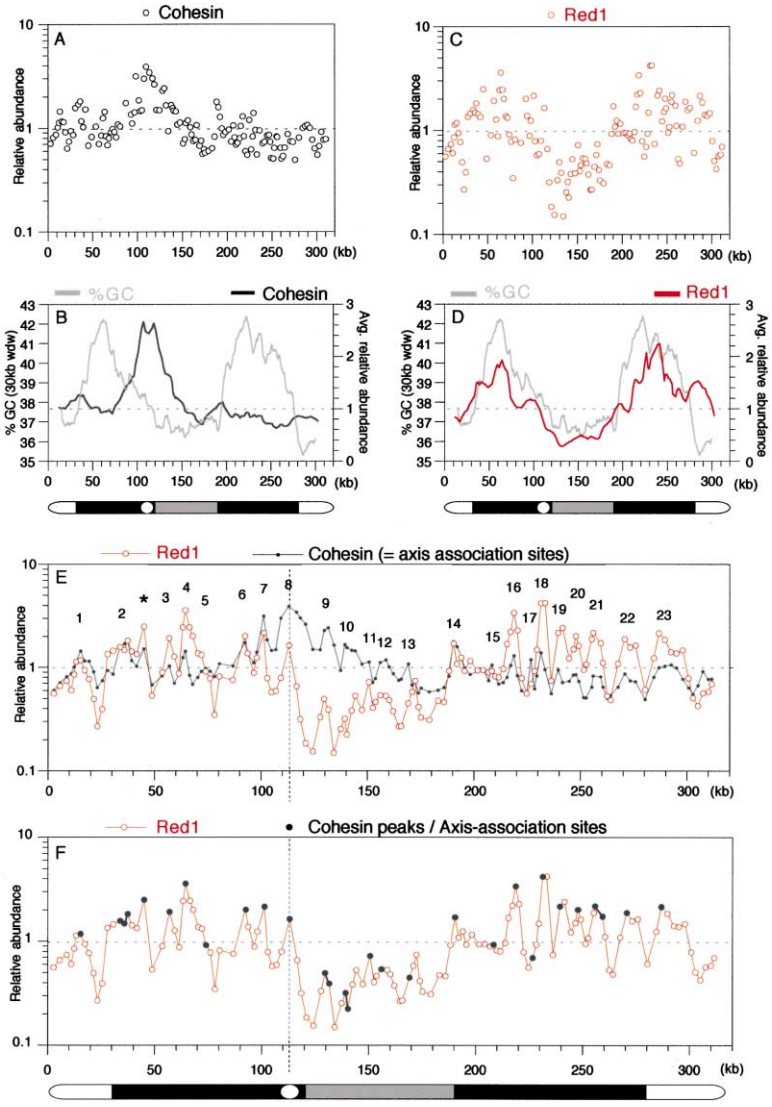

Figure 2. Distribution of Cohesins and Red1 along Chromosome III

(A and C) Low resolution views: relative abundance of Mcd1/Scc1 cohesin in mitotic cells (A; from Figure 2 of Blat and Kleckner, 1999) and of Red1 binding during meiosis (C; average of two experiments) as a function of position along chromosome III.

(B and D) Average base sequence composition (% G+C content averaged over an ~30 kb sliding window; gray line) is compared with similarly averaged relative abundance of cohesin (B, black line) or Red1 (D, red line).

(E and F) High resolution views: local peaks and valleys of relative cohesin binding (connected filled black circles) and relative Red1 binding (connected open red circles) emerge when data points are connected in sequence (E). Peaks of cohesin binding (1–23) are as previously assigned in Blat and Kleckner (1999) plus additional reproducible peak in both cohesin and Red1 distributions (*). Dotted vertical line highlights position of genetically defined minimal centromere. Peaks of cohesin binding (F, filled black circles) define a series of axis-association sites that almost invariably coincide with local maxima of Red1 binding.

Results

Experimental Approach

Red1 and Dmc1 distributions along chromosome III were determined as described (Blat and Kleckner, 1999). In cells proceeding synchronously through meiosis, protein-DNA associations are stabilized by formaldehyde crosslinking. Chromatin is then sheared and fragments associated with the protein of interest isolated by immunoprecipitation. Sheared, immunoprecipitated DNA is then purified and radiolabeled. Absolute and relative abundance of different DNA sequences within the immunoprecipitated sample is determined by hybridization to a membrane containing an array of 133 fragments, ~3 kb long on average, spanning the length of chromosome III. Control hybridizations permit normalization for intrinsic differences in fragment hybridization efficiency.

Red1 Binds along the Length of the Chromosome III Axis but Is Highly Abundant in R-Bands

We previously defined the binding pattern of cohesins (Mcd1/Scc1 and Smc1) along chromosome III in mitotic cells (Blat and Kleckner, 1999). At low resolution, a region of high relative cohesins binding is apparent in ~50 kb surrounding the genetically defined minimal centromere (Figure 2A). This compartment is distinct from R/G-bands (Figure 2B) and might correspond to higher eukaryotic centromeric heterochromatin. At high resolution, a reproducible series of local peaks and valleys of binding emerges (Figure 2E, black line). Peaks correspond to locally AT-rich segments, which in turn define the chromosome axis. Thus, cohesins bind to axis-association sites. Since cohesins also mediate sister chromatid cohesion, these sites are presumably also positions where sister chromatids are connected and thus identify dual loop modules in mitotic cells (see also Guacci et al., 1997).

We have now analyzed the distribution of Red1 along chromosome III using a strain encoding an HA-tagged Red1 protein (NKY3330) at four hours after the onset of meiosis, when DSBs are occurring (Experimental Procedures). Red1 binding is concentrated in two broad peaks corresponding to the two R-bands; the intervening G-band is relatively depleted of Red1, as are chromo-

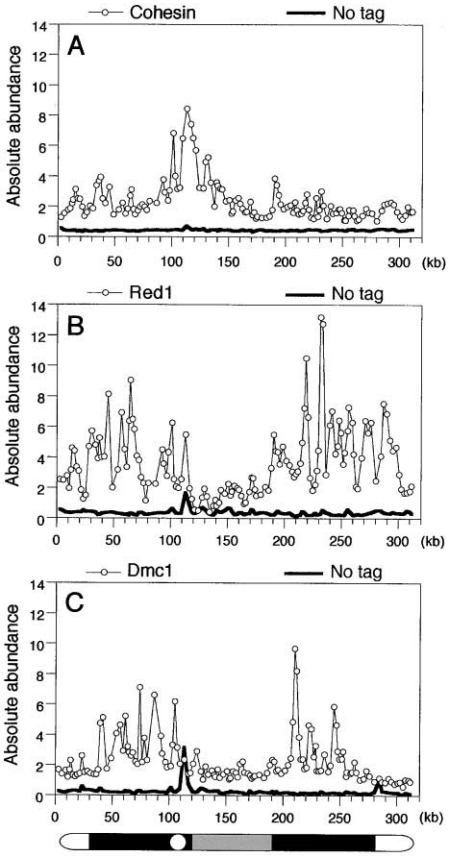

Figure 3. Comparison of ChIP Signals with Signals from Control Strains Lacking Any Epitope Tagged Protein

(A–C) Absolute signal levels for HA-tagged proteins compared with that obtained from isogenic strains lacking any HA epitope.

(A) Analysis of Mcd1/Scc1 cohesin and control mitotic extract; data from experiments shown in Figure 2 of Blat and Kleckner (1999).

(B) Analysis of Red1 and control meiotic extract; Red1 data comes from one of the two experiments averaged in Figure 2.

(C) Analysis of Dmc1 and control meiotic extract; Dmc1 data same as that shown in Figure 6D. Meiotic "no-tag" control data are well below signals obtained from the tagged strains and are relatively flat except for a reproducible signal corresponding to the minimal centromere fragment that is also detected, though not as prominently, in the mitotic control data.

some ends (Figures 2C and 2D). Average base composition and average Red1 distribution, each defined via an ~30 kb sliding window, correspond very closely (Figure 2D). At higher resolution, local peaks and valleys of Red1 binding emerge, analogously to cohesins (Figure 2E). Moreover, despite the differences in their global distributions, Red1 and cohesins bind at the same local positions along the chromosome (Figure 2E): almost every specifically defined cohesins binding site occurs at a local maximum of Red1 binding (Figure 2F; black dots). Thus, meiotic Red1 binds along the entire length of the chromosome III axis at the same axis-association/sister chromatid connection sites defined for mitotic chromosomes. Immunostaining patches of Red1 (Smith and Roeder, 1997) presumably correspond to R-bands, where protein is sufficiently abundant to be detected cytologically. The Red1 binding signal is stronger than that of cohesins; both are well above background as seen in strains lacking any HA-tagged protein (Figures 3A and 3B).

The Red1 binding pattern implies that Red1 localization is determined by the combined inputs of two chromosomal determinants: chromosome axes (versus chromatin loops) and R-band isochores (versus G-bands). This pattern also implies that meiotic chromosomes use the same axis-association/sister cohesion sites as mitotic chromosomes. Accordingly, meiotic cohesin Rec8 (Klein et al., 1999) binds to almost all the same sites as mitotic cohesins and Red1 as shown by genome-wide analysis (J. Gerton, P. Megee, H.G. Yu, J. Derisi, and D. Koshland, personal communication) and PCR analysis of ChIP samples at selected sites (J. Dekker and N.K., unpublished data).

Red1 is several fold more abundant in binding peaks than in intervening valleys (Figures 2E and 2F). This difference likely underestimates the specificity of binding to axis association/cohesion sites because the fragments assayed in the microarray are quite large and sheared probe DNA is heterogeneous. For cohesins, PCR analysis of ChIP samples reveals high specificity binding to short local segments, with little binding to adjacent regions (Tanaka et al., 1999; Laloraya et al., 2000). The total amount of Red1 signal is higher, and the peak/valley differential is greater, than for cohesins (Figure 2E), suggesting even greater binding specificity. ChIP analysis cannot exclude the presence of a small amount of more generally localized Red1 or existence of a Red1 subpopulation that does not crosslink to DNA.

Dmc1 and DSBs Occur in Chromatin Loops, but Also Occur Preferentially in R-Bands

Dmc1 binding was analyzed using a strain expressing HA-tagged Dmc1 (NKY3410). At low resolution, Dmc1 binds prominently in R-bands, less prominently in the G-band, and at very low levels near the chromosome ends (Figure 4A). At high resolution, a reproducible series of ~19 Dmc1 binding peaks and intervening valleys occur fairly regularly along the chromosome, primarily in R-bands (Figure 4D). Dmc1 binding signal is comparable to that of cohesins and well above background (Figure 3C).

The Dmc1 binding pattern is generally similar to that of Red1: preferential R-band abundance with a series of locally defined peaks and valleys. However, direct comparison reveals that the two binding distributions are locally complementary; peaks of Dmc1 binding correspond to valleys of Red1 binding and vice versa. This is most apparent in R-bands where Dmc1 signals are higher (Figures 5A and 5B). Since Red1 binding peaks correspond to axis-association sites, these results imply that Dmc1, and thus DSBs, occur preferentially in chromatin loop sequences. Moreover, the very fact that Dmc1 localizes to a series of specific peaks, plus the fact that those peaks occur at the positions of Red1 valleys, suggests that Dmc1 occurs preferentially in the middles of chromatin loops, i.e., relatively far from the axis-association sites, rather than immediately adjacent to such sites.

These same conclusions can be seen when the Dmc1 distribution is plotted relative to the positions of axis-association sites (defined by the midpoints of their corresponding fragments). Fragments containing peaks of

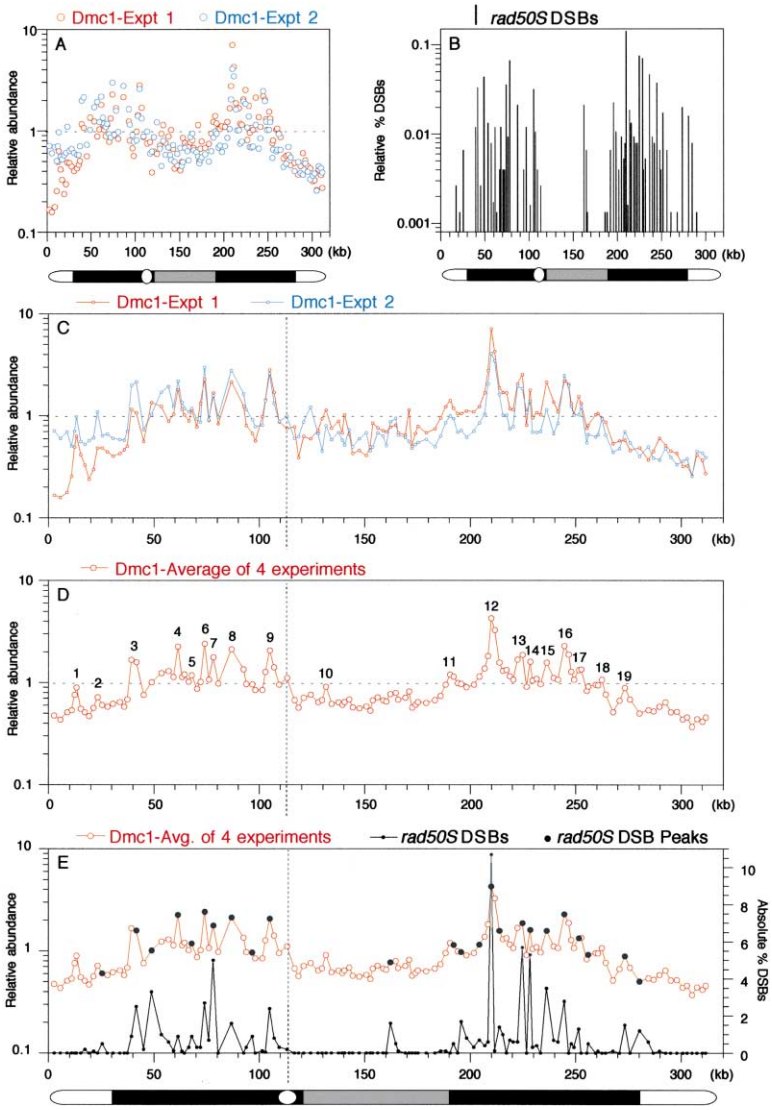

Figure 4. Distributions of Dmc1 and Hotspot DSBs along Chromosome III

(A) Low resolution view of relative Dmc1 abundance determined by ChIP analysis of two independent cultures at 4.5 hr into meiosis (Experiment 1 = open red circles, Experiment 2 = open blue circles).

(B) Distribution of *rad50S* hot spot DSBs (Baudat and Nicolas, 1997) combined over each of the ChIP array fragments used in this study, expressed as a fraction of total DSBs signal, and plotted as a function of chromosomal position (Experimental Procedures).

(C–E) High resolution views of the Dmc1 distribution.

(C) Relative Dmc1 abundance data from (A) are represented as a series of connected circles (Experiment 1 = connected open red circles, Experiment 2 = connected open blue circles).

(D) Relative Dmc1 abundance, the average from four independent experiments (connected open red circles; from C and data not shown), reveals a reproducible series of 19 local peaks.

(E) Average relative Dmc1 abundance (from D) is compared to absolute *rad50S* %DSBs (connected small, black dots); position of peaks of *rad50S* %DSBs are superimposed on the relative Dmc1 abundance curve (large, black dots).

Dmc1 binding nearly all lie between axis association site fragments (Figure 5F). A few fragments contain both types of determinants; however, the peak positions of both cohesins binding and Dmc1 binding could lie anywhere within the relatively large fragments (1–7 kb). Thus, even in these apparent exceptions, Dmc1 probably occurs preferentially at positions other than axis-association sites.

Another view of the chromosome III DSB distribution is provided by direct physical mapping of DSBs at hot spots, analyzed in a mutant where DSBs do not turn over (*rad50S*; Baudat and Nicolas, 1997). This approach does not detect weaker sites; also, the observed distribution may be modulated by effects of the *rad50S* mutation (Borde et al., 2000). Nonetheless, *rad50S* hot spot DSBs exhibit the same general pattern as Dmc1 binding. Globally, hot spot DSBs occur almost exclusively in R-bands (Figure 4B; Baudat and Nicolas, 1997). Locally, when the level of hot spot DSBs is determined for each of the segments represented in the microarray, DSBs are seen to occur in a series of defined peaks, each of which corresponds to a peak of Dmc1 binding (Figure 4E). The hot spot DSBs distribution is again complementary to that of Red1 binding in R-bands (Figures 5C and 5D) and hot spot DSBs occur almost entirely in fragments that do not encode an axis-association site (Figure 5E).

Dmc1 and *rad50S* hot spot DSB distributions do differ in that significant Dmc1 binding is detected in the G-band while hot spot DSBs are virtually absent in this region (compare G-bands with R-bands and chromosome ends; Figure 4A versus 4B; also compare DSB distribution in Figure 4E with Dmc1 distribution in Figure 3C). The Dmc1 distribution is likely more reflective of the actual DSB distribution, as substantial levels of genetic recombination occur in the G-band (Baudat and Nicolas, 1997), presumably via significant levels of DSBs throughout many weaker sites. The *rad50S* mutation may also specifically "disfavor" DSB formation in G-bands (e.g., Borde et al., 2000).

Red1 and R/G-Bands Promote DSB Formation Via Distinct Effects

Red1 is most abundant in regions that exhibit high levels of DSBs (R-bands) and is required for DSB formation. Thus, we wanted to test the possibility that differential

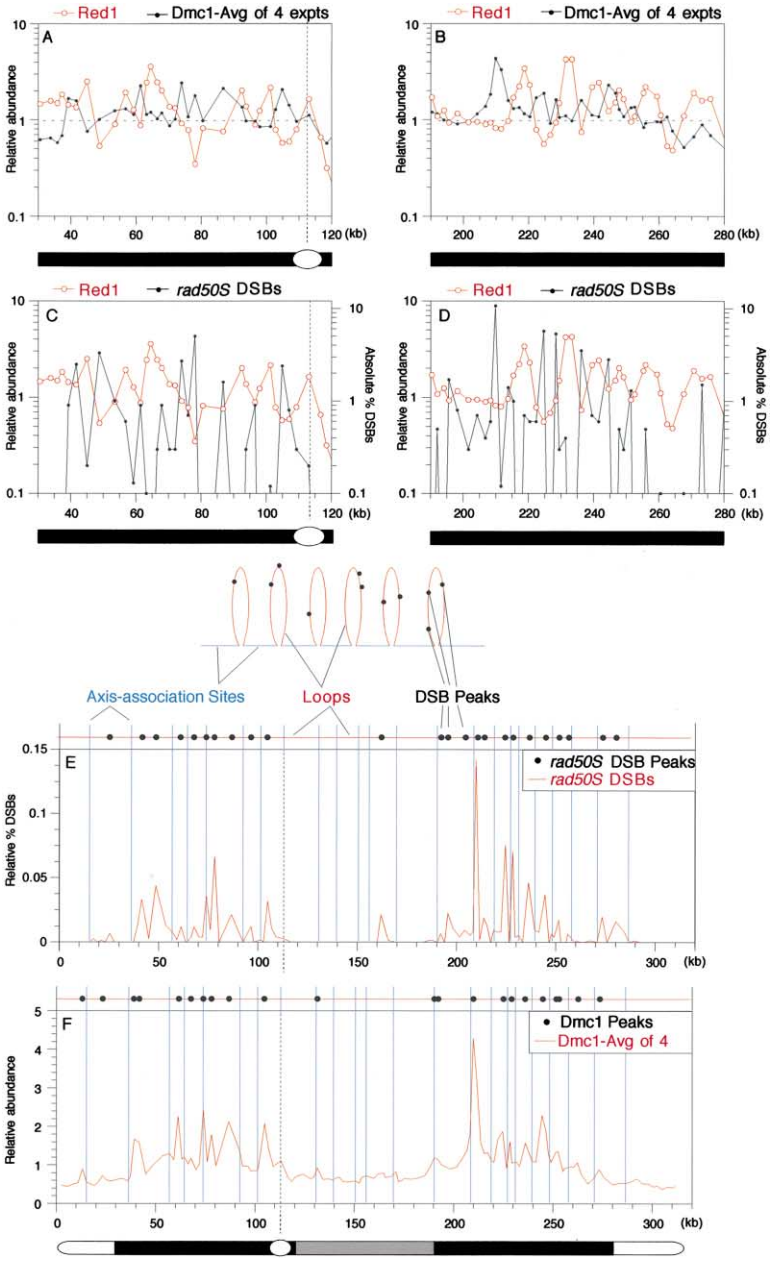

Figure 5. High Resolution Comparisons of the Red1, Dmc1, and *rad50S* DSBs Distributions

(A and B) Relative Red1 abundance compared to relative Dmc1 abundance in the GC-rich isochores (R-bands) on the left (A) and right (B) arms of chromosome III.

(C and D) Relative Red1 abundance compared to meiotic absolute *rad50S* %DSBs in the GC-rich isochores (R-bands) on the left (C) and right (D) arms of chromosome III.

(E and F) Positions of DSB peaks and Dmc1 binding peaks relative to axis-association sites.

Axis-association sites (=cohesin binding peaks, see Figures 2E and 2F) are represented as blue vertical lines. In the interpretative cartoon, these sites are indicated by the blue horizontal line while DSBs and Dmc1 binding peaks are identified as filled black circles. *rad50S* DSB data (E) and Dmc1 data (F) are the same as in Figures 4B and 4D, respectively, but are now graphed on a linear rather than a logarithmic scale.

Red1 abundance is responsible for the R-band biased DSB distribution. To do so, we analyzed the effects of a *red1*Δ mutation on the distribution of DSBs along chromosome III (Figure 6). Chromosomes from synchronous meiotic cultures were resolved by pulsed-field gel electrophoresis; intact chromosome III and DSB-generated fragments were then visualized by Southern hybridization with a probe to the left chromosome end (*CHA1*). Bands of higher mobility than chromosome III represent fragments extending from the probed end to the site of a DSB. The pattern of fragment lengths reveals the pattern of DSBs along the chromosome (Zenvirth et al., 1992).

Dependence of DSB formation on Red1 was analyzed in both *RAD50* and *rad50S* strain backgrounds, each with intrinsic advantages and disadvantages (Results). A common picture emerges: elimination of Red1 reduces DSB levels relatively evenly along chromosome III, similarly in R- and G-bands, in both strain backgrounds (Figures 6A, 6B, and 6C), ≤ 6-fold in both cases (Figures 6E and 6F). This difference is not due to different DSB timing: DSB kinetics are the same in *RED1* and *red1*Δ in both *RAD50* and *rad50S* backgrounds; in both cases, the effects of the *red1*Δ mutation are analogous at all time points (Figure 6A; data not shown; see also Schwacha and Kleckner, 1997; Hunter and Kleckner, 2001).

The same conclusion emerges from analysis of four individual DSB hot spots on three different chromosomes, in both a *rad50S* background and in a *dmc1 rad51* background, where DSB turnover is blocked at a later step (e.g., Schwacha and Kleckner, 1997). In every

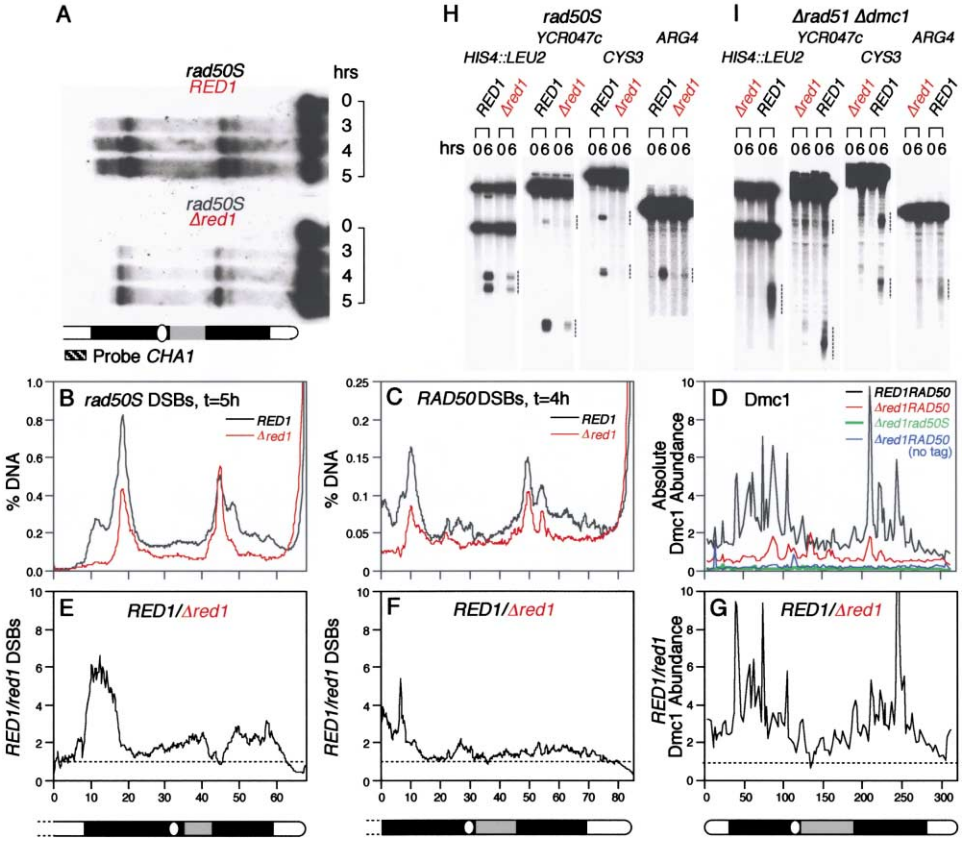

Figure 6. DSB Formation and Dmc1 Binding in the Presence and Absence of Red1

(A) Pulse-field gel analysis of meiotic DSBs along chromosome III in *RED1 rad50S* and *red1*Δ *rad50S* strains.

(B and C) Phosphorimager traces of the t = 5h lanes in A (B) and of the t = 4h lanes for *RED1 RAD50* and *red1*Δ *RAD50* strains (C; gel not shown), from the bottom (left end) to the top (right end) of the gel. DSB levels are calculated as % total hybridizing DNA.

(D) Absolute Dmc1 abundance determined by ChIP analysis in *RED1 RAD50, red1*Δ *RAD50*, and *red1*Δ *rad50S* strains expressing Dmc1-HA, as well as in an untagged *red1*Δ *RAD50* strain. Data from a *RED1 rad50S* strain is very similar to the untagged *red1*Δ *RAD50* strain (not shown).

(E–G) Comparisons of ratios of data from *RED1 rad50S* and *red1*Δ *rad50S* strains (E; from B) and from *RED1 RAD50* and *red1*Δ *RAD50* strains (F and G; from C and D, respectively). Horizontal dotted lines identify a ratio of 1.0.

(H) DSBs at four known hotspot loci in the *rad50S* background, in *RED1* and *red1*Δ. DSB signals are discrete, reflecting absence of 5′-strand resection in *rad50S* strains (Alani et al., 1990). DSB levels as % hybridizing DNA, from left to right, are: 18.0, 3.8, 11.2, 2.6, 7.1, 0.6, 1.6, and 0.3.

(I) DSBs at the same loci analyzed in H but in a *rad51*Δ *dmc1*Δ background, in *RED1* and *red1*Δ. Heterogenous DSB signals reflect hyperresection of 5′-strands in *rad51*Δ *dmc1*Δ strains (e.g., Schwacha and Kleckner, 1997). DSB levels as % hybridizing DNA, from left to right, are: 2.5, 13.1, 3.7, 6.7, 2.5, 6.1, 0.8, and 2.1.

case, elimination of Red1 reduced DSBs levels, 4- to 12-fold in *rad50S* and 2- to 5-fold in *dmc1 rad51* (Figures 6H and 6I). These results are in full accord with previous studies of DSB formation at hot spots in *red1*Δ strains (Schwacha and Kleckner, 1997; Hunter and Kleckner, 2001; Mao-Draayer et al., 1996).

These findings have three important implications. First, DSB formation is functionally dependent upon Red1 all along the chromosome. This is notable given that Red1 occurs prominently along the axis while DSBs occur in chromatin loops. Second, G-band modulation of DSB formation is still observed in the absence of Red1; thus, in contrast to our motivating idea, differences in the relative abundance of Red1 along the chromosome play no functional role for DSB formation. Third, the domainal bias in DSB formation reflects differences between R- and G-bands that are substantially independent of Red1.

R/G-Bands Disfavor Dmc1 Loading and Red1 Counteracts This Effect

The effects of eliminating Red1 on the pattern of Dmc1 binding were examined by parallel Dmc1 ChIP analysis in *RAD50 RED1* and *RAD50 red1*Δ strains (NKY3410 and 3462), as well as in isogenic derivatives carrying the *rad50S* mutation (NKY3463 and 3464). The *rad50S* strains effectively represent negative controls, as Dmc1 does not load onto the unprocessed *rad50S* DSB ends except at extremely low levels (D.K. Bishop, cited in Hunter and Kleckner, 2001). Dmc1 binding signals are much lower in both *rad50S* strains, as well as in a strain lacking any HA-tagged protein, than in either of the *RAD50* strains (Figure 6D), implying that signals in the latter strains represent bona fide Dmc1 binding.

Elimination of Red1 alters both the level and pattern of Dmc1 binding. In a *red1*Δ mutant, total Dmc1 binding signal was reduced by 2.0- and 2.5-fold, in two indepen-

dent experiments. Furthermore, the mutation affects Dmc1 binding in R-bands to a greater extent than in other regions; as a result, Dmc1 now binds relatively evenly along the chromosome, in contrast to the R-band biased distribution observed in wild-type (Figure 6D). This relatively flat Dmc1 binding distribution also contrasts sharply with the R-band-biased distribution of DSBs seen in *red1*Δ (compare red lines in Figures 6B, 6C, and 6D). Taken together these results show that, in the absence of Red1, R-band determinants favor DSB formation but disfavor the loading of Dmc1 onto the ends of those DSBs. Furthermore, in wild-type cells, Red1 is counteracting the otherwise inhibitory effects of R-bands on Dmc1 loading. This is seen most clearly from the ratio of Dmc1 binding in *RED1* and *red1*Δ, which reveals strong peaks of Red1-mediated enhancement specifically in R-bands (Figure 6G). With very few exceptions, Dmc1 signal is more abundant in *RED1* than in *red1*Δ throughout the chromosome (Figure 6G), suggesting that Red1 is required for Dmc1 all along the chromosome but differentially in R-bands.

Discussion

We find that meiotic recombination involves several levels of organizational and functional interplay among basic chromosomal determinants.

Isochore (Chromatin) Status Can Influence Chromosome Axis Status

Red1 localization is determined by the combined effects of two basic chromosomal determinants: axis-association/sister-chromatid cohesion sites and R/G-band isochores. Compartment-specific localization of chromosomal proteins has previously been reported only for specialized regions, e.g., heterochromatin/silenced regions and the rDNA/nucleolus; chromosome axes have not previously been implicated in such a phenomenon.

R-bands and G-bands are characterized by intrinsic differences along the length of the chromatin fiber, e.g., average base composition; also, the R- and G-bands of yeast chromosome III have different physical chromatin fiber properties (Dekker et al., 2002). Thus, the fact that Red1 localizes differentially to the axes in R- and G-bands implies that bulk chromatin status can influence chromosome axis status. Mitotic metaphase chromosomes provide a second example of the same phenomenon: R-bands exhibit straight axes while, in G-bands, axes are helically coiled (Saitoh and Laemmli, 1994).

Chromatin/axis interplay does not appear to involve modulation of basic axis assembly. Yeast axis-association/cohesins binding sites occur with similar density and are used with similar efficiencies in R-bands and G-bands (Blat and Kleckner, 1999); and coiling of mitotic chromosomes arises after axes are fully developed (Gimenez-Abian et al., 1995). Thus, the status of chromatin in developed loops may influence the state of an already developed chromosome axis. Red1 abundance is closely proportional to base composition when averaged over 30–50 kb. Given ~20 kb per yeast meiotic prophase chromatin loop (Moens and Pearlman, 1988), chromatin input into Red1 loading would be averaged over a segment of axis corresponding to ~2–4 loops.

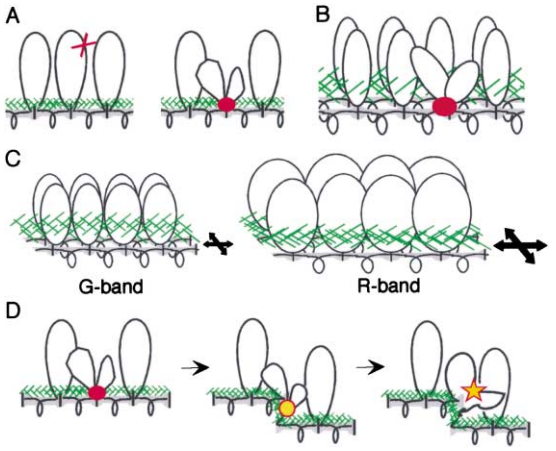

Figure 7. Aspects of Chiasma Formation

(A) Recombination occurs within sequences that are, organizationally, components of chromatin loops (red "X"; left) but are spatially associated with their underlying chromosome axes via their recombinosomes in tethered-loop/axis complexes (red ball; right). Conceptual representation, depicting one homolog only.

(B) An axis-associated recombinosome localized to the base of its chromatin loop (red ball) could comprise a three-way "mark" at the site of recombination along the DNA and at the corresponding site on the chromatid axis underlying that loop, thus also specifically differentiating between sister axes.

(C) Expansion of chromatin loops of meiotic prophase chromosomes could promote axis extension and increased separation of sister chromatid axes, more prominently in R-bands (right) than in G-bands (left).

(D) Logic proposed for a single transition during chiasma formation via linked parallel pathways of events at the DNA and axis levels. Association of the recombinosome with its axis inhibits biochemical progression (left); an underlying axis change occurs (center), triggering a corresponding change at the DNA level (right). The recombinosome changes from an inhibited pretransition configuration (red ball) to a deinhibited pretransition configuration (yellow ball) to a posttransition configuration (yellow star).

Meiotic Recombination Occurs between Chromatin Loops, within Tethered-Loop/Axis Complexes

Dmc1 and DSBs occur preferentially in chromatin loop sequences. Thus, meiotic recombination occurs preferentially between chromatin loops of homologs. DSB formation is already known to be influenced by several other features: "chromatin accessibility" (Wu and Lichten, 1994), base composition isochores (Baudat and Nicolas, 1997; Gerton et al., 2000; this work), and a recently described consensus sequence (Blumental-Perry et al., 2000).

Recombination complexes are in direct physical contact with their chromosome axes at post-DSB stages (Introduction). This study reveals the organizational basis for this association: recombination is occurring between chromatin loop sequences that are tethered to their underlying axes via their recombinosomes (Figures 7A and 7B). These results exclude the alternative possibility, that recombination occurs preferentially in sequences that are immediately adjacent to their axes, i.e., near the bases of chromatin loops (von Wettstein,

1971). Loop tethering has been proposed by van Heemst and Heyting (2000) based on analogies with mitotic DSB repair.

DSB formation is promoted by Red1, which occurs prominently along chromosome axes (Results). This finding seems paradoxical in light of the localization of Dmc1 and DSBs to chromatin loops. One explanation is that recombinosomes become axis-associated prior to the initiation of recombination; DSB formation would then occur within a "tethered-loop/axis" complex, with the axis (e.g., Red1) playing a direct functional role. This possibility is supported by the finding that DSBs occur preferentially at the "tops" of chromatin loops; such bias implies that DSB formation is sensitive to the presence of a loop/axis configuration, e.g., that there is communication between chromosome axes and the recombination process prior to DSB formation. Also, DSB formation is abnormal in mutants lacking either of the other two known meiotic axis-associated proteins: Hop1, which interacts with Red1 (Hollingsworth and Ponte, 1997; Mao-Draayer et al., 1996), and the meiotic cohesin Rec8 (J. Dekker and N.K., unpublished data). Alternatively, low levels of Red1 (and other axis components) could first promote DSB formation and only then mediate axis-association of post-DSB complexes, as during DSB repair (van Heemst and Heyting, 2000).

Domainal Modulation of Recombination

R-band determinants promote DSB formation but disfavor loading of Dmc1 onto DSB ends. R-band chromatin could influence recombinosomes directly and/or could influence axis status and thus, axis-associated recombinosomes. Two considerations point to axis effects at the Dmc1 loading step. First, disfavoring effects of R-band determinants are specifically counteracted by Red1, which is prominently axis-associated. Second, RecA homolog-containing recombinosomes are intimately associated with chromosome axes (Introduction) and mouse Dmc1 protein interacts physically with the axis component, Cor1/SCP3 (Tarsounas et al., 1999). Since Red1 promotes Dmc1 loading, to some degree, also in G-bands, disfavoring effects may also occur in these regions, but to a lesser extent.

Roles of Red1 Protein for Recombination

Red1 is required for DSB formation all along chromosome III and is required after DSB formation to ensure that Dmc1 is loaded onto the ends of those DSBs. Red1 was shown previously to modulate another post-DSB event involving Dmc1: it inhibits onset of stable strand invasion/exchange until Dmc1 has been loaded into the post-DSB recombinosome (Schwacha and Kleckner, 1997; Hunter and Kleckner, 2001). Thus, overall, Red1 mediates the first transition of recombination, promoting first initiation, and then development of the post-DSB recombinosome. Interestingly, DSB catalysis, which is chemically reversible, may actually be driven forward by post-DSB processing steps (Keeney, 2001), with the final level of DSBs being determined by the efficiency of those later steps. Thus, Red1 could potentially exert both its "DSB-formation" and "post-DSB recombinosome" roles by affecting steps that actually occur after chemical formation of a DSB per se, as part of a single coordinate transition.

Given two roles for Red1, a *red1* mutation is predicted to affect the final level of interhomolog recombination in two ways. First, the level of DSBs, and thus interhomolog recombination, will be reduced throughout the genome. Second, failure to load Dmc1 will result in a further decrease, preferentially in R-bands, because this defect causes the DSBs in a *red1* background to engage primarily in inter-sister recombination (Schwacha and Kleckner, 1997; Thompson and Stahl, 1999). *red1* mutations have peculiar genetic effects that match these expectations: (1) interhomolog recombination tends to be more severely reduced at hotter loci, which tend to be in R-bands and are thus subject to both effects; and (2) more severely affected sites tend to exhibit a greater reduction in recombination than attributable to reported effects on DSB levels, in accord with an additional defect (Locus, wild-type recombinant frequency ($\times 10^{-4}$) and ratio of mutant and wild-type frequencies in two studies of *spo13* meiosis: Mao-Draayer et al., 1996: *MET13*-430-.06; *TRP5*-340-0.02; *LEU1*-160-0.04; *HIS7*-12-0.06; *LYS2*-1.4-0.36. Rockmill and Roeder, 1988, 1990: *HIS4*-62-.09; *LEU2*-7-.02; *THR1*-5.1-0.03, *TRP1*-1-0.86).

Red1-R-Band Relationships

During initiation, both R-bands and Red1 work in the same direction to promote DSB formation with effects that are substantially independent; DSBs still occur preferentially in R-bands in the absence of Red1 while Red1 promotes DSB formation all along the chromosomes, similarly in R- and G-bands. During post-DSB steps, R-bands and Red1 work in opposite directions and their effects are compensatory. Dmc1 loading is differentially disfavored in R-bands and Red1 specifically counteracts this tendency. In essence, Red1 function is defined by its role in counteracting R-band effects, suggesting that R-band modulation and Red1 modulation are mechanistically interlinked.

A Physico-Mechanical Mechanism

This study reveals functional interactions between chromosomal components that are in direct physical contact. One explanation for this finding is that recombination is governed by physico-mechanical forces, with functional linkages occurring by direct mechanical linkage.

Interplay among isochores, axes and Red1 suggests a possible basis for such effects. (1) R-band chromatin is thought to be in a more "open" conformation than G-band chromatin (Yokota et al., 1997). Thus, R-band chromatin could be in a more extended state and, correspondingly, a larger volume. Given close packing of chromatin loops along meiotic prophase chromosome axes and close juxtaposition of sister linear-loop arrays, a larger chromatin volume might force chromatid axes along each homolog to be more extended and more separated, thus permitting increased loading of Red1 protein, in proportion to the average base composition within each loop (Figure 7C). (2) A tendency for axis expansion could disfavor (axis-associated) Dmc1 loading; the role of Red1 could be to constrain such expansion, thus counteracting this disfavoring effect. Since

Red1 also promotes Dmc1 loading in the G-band, the same tendency would exist to a lesser degree in that region. (3) The same combination of expansion and constraint can also explain why Red1 is required for normal axis morphogenesis (AE/SC formation) and for maintenance of sister chromatid connections (Introduction). (4) Axis expansion forces may promote recombination initiation by triggering a conformational change in axis-associated pre-DSB recombinosomes. By constraining expansion, Red1 would increase the level of stored expansional force, thus promoting DSB formation. Once a DSB has occurred, the constraining effects of Red1 would protect the developing post-DSB recombinosome from undue effects of expansion.

General Implications for Chiasma Formation

The organizational and functional complexities revealed above can be related to the fact that recombination is part of the integrated process of "chiasma formation", which involves coordinated changes at three levels: (1) exchange between non-sister chromatids at the DNA level; (2) analogous exchange at the chromatid axis level; and (3) local separation of sister chromatid axes (Introduction). When viewed in this context, additional implications emerge.

Tethered-Loop Axis Complexes Provide Three-Way Communication, Thus Providing Spatial and Functional Coordination

Given that DNA exchange occurs between two chromatin loop sequences, accompanying axis-related changes should occur exactly at the bases of the two involved chromatin loops; moreover, changes at all levels must be functionally linked. These requirements can be met by association of recombinosomes with their corresponding chromatid axes, specifically at the bases of their two loops. The result would be a three-way spatial "mark" on each homolog at the site of DNA exchange and at the analogous site of axis exchange, with concomitant differentiation of sister axes at the same positions (Figure 7B). Changes could thus be targeted simultaneously to the appropriate corresponding positions at all three levels. Also, progression at all three levels could be functionally coordinated via direct physical contacts among various components. Domainal effects of bulk chromatin status could then be superimposed upon such ensembles via effects on recombining chromatin sequences and/or via effects on underlying axis status.

Linked Parallel Pathways of Changes at the DNA and Axis Levels

Cytological studies in plants suggest that axes exhibit discontinuities specifically at the sites of axis-associated post-DSB recombinosomes (e.g., Figure 1D; Zickler and Kleckner, 1999). Such morphologies lead to the idea that interruption of DNA via a DSB may be accompanied by interruption of the underlying axis at the corresponding position. The partner homolog axis is then brought into proximity, at which point a matching interruption is also seen on the partner axis. A series of local coordinated changes in both axis and recombinosome morphology then ensue (Albini and Jones, 1987; G.H. Jones, cited in Zickler and Kleckner, 1999).

Such observations, plus the results presented here, lead to the hypothesis that chiasma formation occurs via linked parallel pathways of changes at both DNA and axis levels. At the DNA level, a crossover is known to form via four discrete transitions: (1) an initiating DSB, (2) onset of strand exchange leading to a single-end invasion, (3) completion of strand exchange to give a double Holliday junction, and (4) resolution of the double Holliday junction into products (Hunter and Kleckner, 2001; Allers and Lichten, 2001; V. Boerner, N.H., and N.K., unpublished data). The functional consequences of these steps are initiation, crossover/noncrossover differentiation, final fate-commitment, and completion of recombination (Hunter and Kleckner, 2001). Axis exchange and separation of sister axes might proceed by four functionally analogous steps. For example, DSB formation would represent not only initiation at the DNA level but, more generally, initiation of chiasma formation, at both DNA and axis levels, with interruptions occurring at corresponding positions both within the DNA and specifically along the involved chromatids, and with resulting local differentiation between sister axes (e.g., Figure 7D).

Local Axis Changes Govern Local DNA Changes

We further suggest that, at each step, a local change in axis status is determinative for (i.e., "triggers") progression of DNA events. For example, if pre-DSB recombinosomes are axis associated, a local structural transition in the chromosome axes might (1) initiate chiasma formation at the axis level; (2) concomitantly ensure irreversibility of a DSB by changing the conformation of Spo11 protein (Keeney, 2001); and (3) prepare the site for development of an axis-associated post-DSB recombinosome (Figure 7D). Such logic could help to explain the key roles of axis components in chiasma formation. Also, the phenomenon of "crossover interference" requires communication along chromosomes such that occurrence of an event at one site affects occurrence of events at nearby sites. Most interference models assume that such communication occurs by transmission of information along the axes (e.g., Egel, 1978; King and Mortimer, 1990; Sym and Roeder, 1994; Zickler and Kleckner, 1998; Kaback et al., 1999). An implicit assumption of such models is that chromosome axis status can govern the status of axis-associated DNA recombination complexes.

Linking Mitotic and Meiotic Chromosome Function

Meiotic recombination appears to have evolved from mitotic DSB repair (Van Heemst and Heyting, 2000). Axis destabilization and sister separation appear to occur locally at sites of meiotic chiasmata (Introduction). These same processes occur globally along mitotic (and meiotic) chromosomes, as seen for axial coiling at prometaphase, axis disintegration during telophase, and progressive sister separation from prometaphase through anaphase. Thus, during meiosis, the global structural changes of the mitotic program could be targeted specifically to relevant local sites by axis-association of recombinosomes where, in turn, they could govern the progression of events at the DNA/recombinosome level.

Experimental Procedures

Strains

NKY3299 is *leu2::hisG/" MATa/MATα ura3/" arg4-bgl/arg4-nsp lys2/"ho::hisG/"*. Isogenic derivatives of NKY3299 are NKY3330 (*RED1-1XHA::URA3/"*) and NKY3410 (*DMC1-3XHA::kanMX4/DMC1*). Both epitope tags are located at the C terminus and both strains exhibit normal levels of spore formation and spore viability (data not shown). Isogenic derivatives of NKY3410 are NKY3462 (*red1Δ*), NKY3463 (*rad50S*/KI81; Alani et al., 1990), and NKY3464 (*red1Δ rad50S*). Isogenic derivatives of NKY3299 are NKY3302 (*red1Δ*), NKY3424 (*rad50S*), and NKY3425 (*red1Δ rad50S*).

NKY3230 is *HIS4::LEU2-(NBam)/his4-X::LEU2-(NBam)-URA3 leu2::hisG/"MATa/MATα ho::hisG/" ura3(ΔPst-Sma)/"*. Isogenic derivatives of NKY3230 are NHY493 (*rad50S*), NHY1131 (*rad50S Δred1::kanMX4*), NHY1066 (*Δrad51::hisG Δdmc1::kanMX4*), and NHY 1063 (*Δrad51::hisG Δdmc1::kanMX4 Δred1::kanMX4*) (Shinohara et al., 1992; Hunter and Kleckner, 2001).

ChIP Experiments

Distributions of Red1 and Dmc1 along chromosome III were analyzed as described by Blat and Kleckner (1999) and http://www.mcb.harvard.edu/kleckner/ChIP.html. The hybridization signal for each fragment on the filter was measured with a phosphorimager and general filter background was subtracted to give a primary ChIP value (PC). A parallel hybridization was performed with DNA prepared identically except that immunoprecipitation was omitted and analyzed like the ChIP sample to give a primary Non-ChIP value (PNC). The PNC controls for intrinsic differences in hybridization efficiencies among the various fragments. The PC and PNC data were then compared in one of three ways. (1) "Absolute Abundance": for every fragment, each PC is divided by the corresponding NPC and the resulting ratios are plotted as a function of chromosomal position. Values for absolute abundance are reproducible from experiment to experiment and are useful in analyzing differences in the amount of signal obtained from different strain backgrounds. (2) "Relative Abundance": for every fragment, each PC is first expressed as a fraction of the sum of all the PCs; each NPC signal is expressed analogously. The ratio of these two fractions is then plotted as a function of chromosomal position. This approach reports relative abundance of a protein along the chromosome and eliminates noise from small residual differences in absolute abundance. (3) 30 kb sliding window analysis: broad base composition isochores are detected using a 30 kb-sliding window (Baudat and Nicolas, 1997; Sharp and Lloyd, 1993; Dujon, 1996). Average protein binding is examined in an analogous way by averaging relative abundance over a sliding window of nine adjacent probed fragments (28.5 ± 3.7 kb). Each average value was then plotted at the position of the central fragment.

Representation of *rad50S* DSB Levels

Baudat and Nicolas (1997) reported the levels of meiotic DSBs at detectable hot spots along chromosome III. To compare this data directly with ChIP data, we calculated the total level of hot spot DSBs observed within each fragment in the ChIP array. These levels were then plotted analogously to ChIP data (PC/NPC ratios) either (1) directly as "Absolute % DSBs"; (2) after dividing by the sum of the values for all fragments, as "Relative % DSBs"; or (3) as "Average relative % DSBs", averaged over a nine-fragment sliding window. The DSBs originally reported in the coding region of *GLK1* (Baudat and Nicolas, 1997) have been subtracted from this analysis as they have subsequently been found be an artifact of the DNA extraction method (A. Nicolas and F. Baudat, personal communication).

Synchronous Meiosis and Analysis of Other Meiotic Events

For ChIP studies, cultures were induced to undergo synchronous meiosis as described (Alani et al., 1990) except that the YPD and YPA media contained Uracil (20 mg/L), Arginine (20 mg/L), Leucine (100 mg/L), and Lysine (30 mg/L) and SPM medium contained Uracil (4 mg/L), Arginine (4 mg/L), Leucine (20 mg/L), and Lysine (6 mg/L). YPA cultures contained Antifoam 289 (0.01%, Sigma). A total of 500–1000 ml of culture was processed per ChIP sample. Due to the large culture volumes required, meiosis is slightly slower than optimal; e.g., DSBs peak after ~4 hr rather than ~3 hr as in Hunter and Kleckner (2001). PFG analysis of DSBs was performed according to Borde et al. (2000). DSBs at individual loci were analyzed as in Hunter and Kleckner (2001).

Previous *red1* DSB Studies

In one study, we reported that DSBs formed at wild-type levels in a *red1 rad50S* mutant (Xu et al., 1997). The discrepancy with current results reflects an artifact resulting from the DNA extraction procedure used in the previous study. However, this artifact is likely to be meaningful. We suggested that all recombinosomes exist in a "poised" form in a *red1* strain and that "extra" DSBs can arise, e.g., via detergent activation of Spo11 topoisomerase cleavage (Xu et al., 1997) or, it could now be suggested, by providing accessibility to the endogenous activity of Nuc1, a mitochondrial nuclease released under some conditions (Debrauwère et al., 1999). The level of DSBs observed would thus be a readout of the total number of assembled recombinosomes.

Acknowledgments

We thank Denise Zickler for allowing us to publish her photographs of rye chromosomes. We also thank Charles Tease, MacMillan Publishers Ltd., Cambridge University Press, and the Botanical Society of America for allowing us to reproduce previously published photographs. This work was supported by a grant to N.K. from the National Institutes of Health (ROI-GM44794). R.U.P. is supported by a National Science Foundation Minority Postdoctoral Research Fellowship.

Received: June 27, 2002
Revised: October 30, 2002

References

Alani, E., Padmore, R., and Kleckner, N. (1990). Analysis of wild-type and *rad50* mutants of yeast suggests an intimate relationship between meiotic chromosome synapsis and recombination. Cell *61*, 419–436.

Albini, S.M., and Jones, G.H. (1987). Synaptonemal complex spreading in *Allium cepa* and *A. fistulosum*. I. The initiation and sequence of pairing. Chromosoma *95*, 324–338.

Allers, T., and Lichten, M. (2001). Differential timing and control of noncrossover and crossover recombination during meiosis. Cell *106*, 47–57.

Anderson, L.K., Offenberg, H.H., Verkuijlen, W.M., and Heyting, C. (1997). RecA-like proteins are components of early meiotic nodules in lily. Proc. Natl. Acad. Sci. USA *94*, 6868–6873.

Bailis, J.M., and Roeder, G.S. (1998). Synaptonemal complex morphogenesis and sister-chromatid cohesion require Mek1-dependent phosphorylation of a meiotic chromosomal protein. Genes Dev. *12*, 3551–3563.

Baudat, F., and Nicolas, A. (1997). Clustering of meiotic double-strand breaks on yeast chromosome III. Proc. Natl. Acad. Sci. USA *94*, 5213–5218.

Blat, Y., and Kleckner, N. (1999). Cohesins bind to preferential sites along yeast chromosome III, with differential regulation along arms versus the centric region. Cell *98*, 249–259.

Blumental-Perry, A., Zenvirth, D., Klein, S., Onn, I., and Simchen, G. (2000). DNA motif associated with meiotic double-strand break regions in *Saccharomyces cerevisiae*. EMBO Rep. *1*, 232–238.

Borde, V., Goldman, A.S., and Lichten, M. (2000). Direct coupling between meiotic DNA replication and recombination initiation. Science *290*, 806–809.

Debrauwère, H., Buard, J., Tessier, J., Aubert, D., Vergnaud, G., and Nicolas, A. (1999). Meiotic instability of human minisatellite CEB1 in yeast requires DNA double-strand breaks. Nat. Genet. *23*, 367–371.

Dekker, J., Rippe, K., Dekker, M., and Kleckner, N. (2002). Capturing chromosome conformation. Science *295*, 1306–1311.

Dresser, M.E., and Giroux, C.N. (1988). Meiotic chromosome behavior in spread preparations of yeast. J. Cell Biol. *106*, 567–573.

Dujon, B. (1996). The yeast genome project: what did we learn? Trends Genet. *12*, 263–270.

Egel, R. (1978). Synaptonemal complex and crossing-over: structural support or interference? Heredity *41*, 233–237.

Franklin, A.E., McElver, J., Sunjevaric, I., Rothstein, R., Bowen, B., and Cande, W.Z. (1999). Three-dimensional microscopy of the Rad51 recombination protein during meiotic prophase. Plant Cell *11*, 809–824.

Gerton, J.L., DeRisi, J., Shroff, R., Lichten, M., Brown, P.O., and Petes, T.D. (2000). Inaugural article: global mapping of meiotic recombination hotspots and coldspots in the yeast *Saccharomyces cerevisiae*. Proc. Natl. Acad. Sci. USA *97*, 11383–11390.

Gimenez-Abian, J.F., Clarke, D.J., Mullinger, A.M., Downes, C.S., and Johnson, R.T. (1995). A postprophase topoisomerase II-dependent chromatid core separation step in the formation of metaphase chromosomes. J. Cell Biol. *131*, 7–17.

Guacci, V., Koshland, D., and Strunnikov, A. (1997). A direct link between sister chromatid cohesion and chromosome condensation revealed through the analysis of *MCD1* in *S. cerevisiae*. Cell *91*, 47–57.

Hollingsworth, N.M., and Ponte, L. (1997). Genetic interactions between *HOP1*, *RED1* and *MEK1* suggest that MEK1 regulates assembly of axial element components during meiosis in the yeast *Saccharomyces cerevisiae*. Genetics *147*, 33–42.

Holmquist, G.P. (1992). Chromosome bands, their chromatin flavors, and their functional features. Am. J. Hum. Genet. *51*, 17–37.

Hunter, N., and Kleckner, N. (2001). The single-end invasion: an asymmetric intermediate at the double-strand break to double-holliday junction transition of meiotic recombination. Cell *106*, 59–70.

John, B. (1990). Meiosis (New York: Cambridge University Press).

Kaback, D.B., Barber, D., Mahon, J., Lamb, J., and You, J. (1999). Chromosome size-dependent control of meiotic reciprocal recombination in *Saccharomyces cerevisiae*: the role of crossover interference. Genetics *152*, 1475–1486.

Keeney, S. (2001). Mechanism and control of meiotic recombination initiation. Curr. Top. Dev. Biol. *52*, 1–53.

King, J.S., and Mortimer, R.K. (1990). A polymerization model of chiasma interference and corresponding computer simulation. Genetics *126*, 1127–1138.

Klein, F., Mahr, P., Galova, M., Buonomo, S.B., Michaelis, C., Nairz, K., and Nasmyth, K. (1999). A central role for cohesins in sister chromatid cohesion, formation of axial elements, and recombination during yeast meiosis. Cell *98*, 91–103.

Laloraya, S., Guacci, V., and Koshland, D. (2000). Chromosomal addresses of the cohesin component Mcd1p. J. Cell Biol. *151*, 1047–1056.

Mao-Draayer, U., Galbraith, A.M., Pittman, D.L., Cool, M., and Malone, R.E. (1996). Analysis of meiotic recombination pathways in the yeast *Saccharomyces cerevisiae*. Genetics *144*, 71–86.

Moens, P.B., and Pearlman, R.E. (1988). Chromatin organization at meiosis. Bioessays *9*, 151–153.

Pelttari, J., Hoja, M.R., Yuan, L., Liu, J.G., Brundell, E., Moens, P., Santucci-Darmanin, S., Jessberger, R., Barbero, J.L., Heyting, C., and Hoog, C. (2001). A meiotic chromosomal core consisting of cohesin complex proteins recruits DNA recombination proteins and promotes synapsis in the absence of an axial element in mammalian meiotic cells. Mol. Cell. Biol. *21*, 5667–5677.

Petes, T.D. (2001). Meiotic recombination hot spots and cold spots. Nat. Rev. Genet. *2*, 360–369.

Rockmill, B., and Roeder, G.S. (1990). Meiosis in asynaptic yeast. Genetics *126*, 563–574.

Rockmill, B., and Roeder, G.S. (1988). *RED1*: a yeast gene required for the segregation of chromosomes during the reductional division of meiosis. Proc. Natl. Acad. Sci. USA *85*, 6057–6061.

Saitoh, Y., and Laemmli, U.K. (1994). Metaphase chromosome structure: bands arise from a differential folding path of the highly AT-rich scaffold. Cell *76*, 609–622.

Schwacha, A., and Kleckner, N. (1997). Interhomolog bias during meiotic recombination: meiotic functions promote a highly differentiated interhomolog-only pathway. Cell *90*, 1123–1135.

Sharp, P.M., and Lloyd, A.T. (1993). Regional base composition variation along yeast chromosome III: evolution of chromosome primary structure. Nucleic Acids Res. *21*, 179–183.

Shinohara, A., Ogawa, H., and Ogawa, T. (1992). Rad51 protein involved in repair and recombination in *S. cerevisiae* is a RecA-like protein. Cell *69*, 457–470.

Shinohara, M., Gasior, S.L., Bishop, D.K., and Shinohara, A. (2000). Tid1/Rdh54 promotes colocalization of Rad51 and Dmc1 during meiotic recombination. Proc. Natl. Acad. Sci. USA *97*, 10814–10819.

Smith, A.V., and Roeder, G.S. (1997). The yeast Red1 protein localizes to the cores of meiotic chromosomes. J. Cell Biol. *136*, 957–967.

Stack, S.M., and Anderson, L.K. (1986). Two-dimensional spreads of synaptonemal complexes from solanaceous plants. II. Synapsis in *Lycopersicon esculentum* (tomato). Am. J. Bot. *73*, 264–281.

Sym, M., and Roeder, G.S. (1994). Crossover interference is abolished in the absence of a synaptonemal complex protein. Cell *79*, 283–292.

Tanaka, T., Cosma, M.P., Wirth, K., and Nasmyth, K. (1999). Identification of cohesin association sites at centromeres and along chromosome arms. Cell *98*, 847–858.

Tarsounas, M., Morita, T., Pearlman, R.E., and Moens, P.B. (1999). RAD51 and DMC1 form mixed complexes associated with mouse meiotic chromosome cores and synaptonemal complexes. J. Cell Biol. *147*, 207–220.

Tease, C. (1978). Cytological detection of crossing-over in BUdR substituted meiotic chromosomes using the fluorescent plus Giemsa technique. Nature *272*, 823–824.

Thompson, D.A., and Stahl, F.W. (1999). Genetic control of recombination partner preference in yeast meiosis. Isolation and characterization of mutants elevated for meiotic unequal sister-chromatid recombination. Genetics *153*, 621–641.

van Heemst, D., and Heyting, C. (2000). Sister chromatid cohesion and recombination in meiosis. Chromosoma *109*, 10–26.

von Wettstein, D. (1971). The synaptonemal complex and four-strand crossing over. Proc. Natl. Acad. Sci. USA *68*, 851–855.

Wu, T.C., and Lichten, M. (1994). Meiosis-induced double-strand break sites determined by yeast chromatin structure. Science *263*, 515–518.

Xu, L., Weiner, B.M., and Kleckner, N. (1997). Meiotic cells monitor the status of the interhomolog recombination complex. Genes Dev. *11*, 106–118.

Yokota, H., Singer, M.J., van den Engh, G.J., and Trask, B.J. (1997). Regional differences in the compaction of chromatin in human H0/G1 interphase nuclei. Chromosome Res. *5*, 157–166.

Zenvirth, D., Arbel, T., Sherman, A., Goldway, M., Klein, S., and Simchen, G. (1992). Multiple sites for double-strand breaks in whole meiotic chromosomes of *Saccharomyces cerevisiae*. EMBO J. *11*, 3441–3447.

Zickler, D., and Kleckner, N. (1998). The leptotene-zygotene transition of meiosis. Annu. Rev. Genet. *32*, 619–697.

Zickler, D., and Kleckner, N. (1999). Meiotic chromosomes: integrating structure and function. Annu. Rev. Genet. *33*, 603–754.